

SOT-MRAM Elements Based on Spin Hall Effect: Macrospin Model of Two-Step Switching Control

© N.V. Ostrovskaya, V.A. Skidanov, Yu.A. Iusipova

Institute for Design Problems in Microelectronics of Russian Academy of Sciences, Zelenograd, Moscow, Russia
e-mail: ost.ippm@yandex.ru

Received November 22, 2022

Revised January 20, 2023

Accepted February 10, 2023

The article presents the results of a qualitative study of the model of a modern magnetic memory cell, in which the spin Hall effect is used for recording. Cells of square cross-section with longitudinal anisotropy of the active layer are considered. Based on the Landau–Lifshitz–Gilbert vector equation, a mathematical model for controlling the process of writing zero and one into a cell is constructed. In the approximation of a uniform distribution of magnetization, a system of equations is derived that describes the dynamics of magnetization under the action of a magnetic field and spin current. The parameters of the qualitatively equivalent dynamics of the model are determined. It has been established that at zero currents and fields in both cases there are two main stable equilibrium positions. These equilibria, depending on the mutual orientation of the magnetization vector of the active and reference layers, correspond to zero and one, written in the cell. The transition from one cell state to another is described by solving a system of differential equations. A bifurcation diagram of a dynamical system in the variables „field–current“ is constructed. It is shown that with a given configuration of the memory element, external influences transfer the magnetization to an intermediate state in the plane of the free layer, which, when the current and field are turned off, leads to writing zero or one to the memory cell. The critical switching current is estimated as a function of the applied external magnetic field.

Keywords: spintronics, orbitronics, magnetization, Landau–Lifshitz–Gilbert equation, spin Hall effect, spin current, charge current, spin torque, longitudinal anisotropy, planar anisotropy.

DOI: 10.21883/TP.2023.05.56071.250-22

Introduction

The effect of magnetization control in a thin ferromagnetic film using spin-orbital torque (SOT) generated by a flow of moving electrons is an alternative to magnetization control using spin-transfer torque (STT). This effect is of great interest in connection with its applications in the magnetic random-access memory (MRAM) technology (see, for example, review [1]). Compared to STT-MRAM, the use of SOT can additionally lower the power consumption of the memory device, increase the speed and wear resistance, which makes it an ideal candidate for use in an embedded RAM or a computer cache memory. These perspectives stimulate R&D of both the physics of the SOT effect (see overview [2]) and the corresponding devices using the SOT effect (for example, [3]). The advantages of SOT-MRAM in comparison with STT-MRAM became obvious already at the stage of pilot studies, namely separate circuits for reading and writing information and a symmetrical scheme for recording zero and one, which the cells of STT-MRAM lacked.

Much attention during SOT studies is paid to the study of materials that demonstrate high efficiency of converting charge current into spin current (SOT efficiency), as well

as the development of suitable layered structures with their application. Such materials as topological insulator $\text{Bi}_x\text{Se}_{1-x}$ or alloys $\text{Pt}_{1-x}\text{Au}_x$, which have spin-Hall angles larger than unit and high spin-Hall conductivity, are of great interest for this purpose in addition to heavy metals Pt, Ta and W [4–6]. Several variants of SOT-MRAM schemes with an in-plane or perpendicular magnetic anisotropy [7] were proposed for the second purpose. A mathematical model of a SOT-MRAM memory element with an in-plane anisotropy of the free layer placed in a magnetic field parallel to the axis of light magnetization is investigated in this paper. This configuration differs from those discussed in [7].

1. Mathematical model of the SOT-MRAM element based on the spin Hall effect

The SOT-MRAM memory element considered here consists of an active ferromagnetic layer (FL — free layer), which is sandwiched between a conductive busbar and an insulator layer (tunnel barrier — TB), a reference layer (PL — pinned layer) with fixed magnetization is located above the insulator. The recording current I_c is passed through the HM (HM-heavy metal) bus in one direction

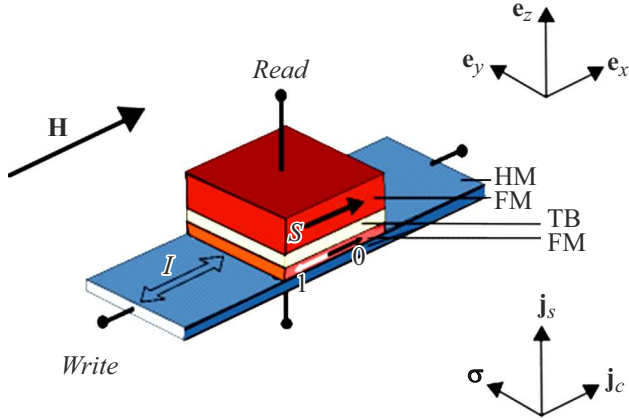


Figure 1. Geometry of the SOT-MRAM model with the in-plane anisotropy of the free layer. The external magnetic field \mathbf{H} is co-directed with the anisotropy field. The values of the geometric dimensions of the element used in calculation: the thickness of the active layer $d = 5$ nm, the cross-sectional area of the element $S = 10 \times 10$ nm.

or the other, depending on whether zero or one is being recorded. The reading current is passed perpendicular to the plane of the layers. Depending on the relative position of the axis of light magnetization of ferromagnetic layers and the current density vector, several types of SOT-MRAM elements can be distinguished — X -, Y - and Z -types with different operating and critical characteristics of [7]. A common design feature of the three elements considered in [7] is the orthogonality of the direction of the external field to the anisotropy axis of the active ferromagnetic layer. However, these types do not exhaust all possible options for the relative location of the external field, the axis of anisotropy and the direction of electron flow. Figure 1 schematically shows the configuration of the element considered in this paper. The anisotropy axis of the free layer material is parallel to the external magnetic field \mathbf{H} .

The dynamics of the magnetization vector in the free layer is described by the Landau-Lifshitz-Gilbert vector equation — (LLG) [8,9]:

$$\frac{\partial \mathbf{M}}{\partial t} = -|\gamma|\mu_0[\mathbf{M} \times \mathbf{H}_{\text{eff}}] + \frac{\alpha}{M_s} \left[\mathbf{M} \times \frac{\partial \mathbf{M}}{\partial t} \right] + \mathbf{T}_{\text{SOT}}. \quad (1)$$

Here $\mu_0 = 4\pi \cdot 10^{-7}$ N/A² is the vacuum magnetic permeability, γ is the gyromagnetic ratio: $\gamma = g\mu_B/\hbar = 1.76 \cdot 10^{11}$ T⁻¹ · s⁻¹, α is the dimensionless dissipation coefficient, M_s is the saturation magnetization, \mathbf{H}_{eff} is the effective magnetic field reflecting those types of physical interactions that are taken into account in the model. In the monodomain approximation

$$\mathbf{H}_{\text{eff}} = \mathbf{H} + \mathbf{H}_f + \mathbf{H}_a,$$

where \mathbf{H} is the external magnetic field, $\mathbf{H}_f = -M_z \mathbf{e}_z$ is the effective demagnetization field, $\mathbf{H}_a = 2K_a \mathbf{e}_x$ is the effective magnetic anisotropy field. The last term in the

equation (1) is the rotational magnetic moment (torque) acting on the magnetization of the free layer from the spin-polarized Hall current. The effective magnetic field of the exchange interaction will be considered negligible (the Stoner-Wohlfarth approximation). The moment of force acting on the magnetization in the free layer can be decomposed into three components. One of these components coincides with the direction of magnetization, i.e., creates zero rotational moment, the other two are mutually orthogonal and are written as follows:

$$\begin{aligned} \mathbf{T} = \mathbf{T}_{\text{FL}} + \mathbf{T}_{\text{DL}} = & |\gamma\mu_0|j\theta_{\text{SH}}\chi_{\text{DL}}[\mathbf{M} \times [\mathbf{M} \times \mathbf{e}_y]] \\ & + |\gamma\mu_0|j\theta_{\text{SH}}\chi_{\text{FL}}M_s[\mathbf{M} \times \mathbf{e}_y], \end{aligned} \quad (2)$$

where

$$j = \theta_{\text{SH}}\eta J/J_{\text{norm}}, \quad J_{\text{norm}} = \frac{dg|e|\mu_0 M_s^2}{\hbar},$$

J — charge current density, d — free layer thickness, μ_B — Bohr magneton, g — factor Lande, e — electron charge, $\theta_{\text{SH}} = j_s/j_c$ — spin-Hall coefficient of efficiency characterizing the ratio of vertical spin current density to horizontal charge current density (spin-Hall effect angle), $\eta < 1$ — polarization efficiency coefficient (the characteristic of the insulating layer). Typical values of the spin Hall effect angle lie in the range 0.3–0.4 [10]. In our calculations we put $\eta\theta_{\text{SH}} = 0.4$. The ratio J/J_{norm} is a dimensionless value of the control charge current j_c . Note the difference in the direction of spin polarization in this case and in STT-MRAM with longitudinal anisotropy, considered earlier in [11–13]: here the spins are oriented along the direction \mathbf{e}_y perpendicular to the direction of the free layer anisotropy field, whereas in the case of STT-MRAM with the same configuration of the elements the spins are polarized along the direction \mathbf{e}_x . The first term in the expression (2) is the damping component of the rotational moment created by spin-polarized electrons, the second term is the field component. The influence of the field component on the critical switching characteristics was considered in work [14].

The normalizations transform equation (1) to a dimensionless form

$$\frac{\partial \mathbf{m}}{\partial \tilde{t}} = -[\mathbf{m} \times \mathbf{h}_{\text{eff}}] + \alpha \left[\mathbf{m} \times \frac{\partial \mathbf{m}}{\partial \tilde{t}} \right] + \mathbf{t}, \quad (3)$$

where $\mathbf{h}_{\text{eff}} = \mathbf{H}_{\text{eff}}/M_s$, $\mathbf{t} = \mathbf{T}/\gamma\mu_0 M_s^2$, $\mathbf{m} = \mathbf{M}/M_s$, $|\mathbf{m}| = 1$ time \tilde{t} is measured in units of $(\gamma\mu_0 M_s)^{-1}$. Here $\mathbf{h}_{\text{eff}} = \mathbf{h}_{\text{app}} + \mathbf{h}_a + \mathbf{h}_f$. In the case of an external field \mathbf{h}_{app} directed along the axis OX , the summand has the form $\mathbf{h}_{\text{app}} = h\mathbf{e}_x$. The effective anisotropy field in this model is also oriented along OX

$$\mathbf{h}_a = k(\mathbf{m}, \mathbf{e}_x)\mathbf{e}_x = km_x \mathbf{e}_x,$$

where $k = 2K_a\mu_0^{-1}M_s^{-2}$, K_a is the magnetic anisotropy constant. In calculations, we used a normalized dimensionless

cobalt anisotropy coefficient equal to 0.43. The demagnetization field \mathbf{h}_f is determined by the ratio $\mathbf{h}_f = -\hat{\mathbf{q}}\mathbf{m}$, where the tensor $\hat{\mathbf{q}}$ is the demagnetization form factor. It can be assumed that in the geometry of a square-section memory element the tensor $\hat{\mathbf{q}}$ has only one non-zero component in the last line on the main diagonal and, consequently, the demagnetization field has the form $\mathbf{h}_f = -m_z \mathbf{e}_z$. Thus, the effective magnetic field in the normalized Landau–Lifshitz equation for this configuration will be equal to

$$\mathbf{h}_{\text{eff}} = \mathbf{h}_{\text{app}} + \mathbf{h}_a + \mathbf{h}_f = (h + km_x)\mathbf{e}_x - m_z \mathbf{e}_z.$$

2. Dynamical system

Let us rewrite equation (3) in the form of

$$\frac{\partial \mathbf{m}}{\partial \tilde{\tau}} = -[\mathbf{m} \times (\mathbf{h}_{\text{eff}} - bjm_y \mathbf{e}_y - bje_y)] + \alpha \left[\mathbf{m} \times \frac{\partial \mathbf{m}}{\partial \tilde{\tau}} \right] \quad (4)$$

and introduce a new effective field vector that takes into account the effect of the spin-Hall current:

$$\mathbf{f} = \mathbf{h}_{\text{eff}} - bjm_y \mathbf{e}_y - bje_y = (h + km_x + bjm_z)\mathbf{e}_x - bje_y + (-bjm_x - m_z)\mathbf{e}_z.$$

Next, we solve the Landau-Lifshitz-Gilbert equation with respect to the time derivative and obtain its expression in the normal form:

$$\frac{\partial \mathbf{m}}{\partial \tau} = -[\mathbf{m} \times \mathbf{f}] + \alpha \mathbf{f} - \alpha \mathbf{m}(\mathbf{m}, \mathbf{f}). \quad (5)$$

The equation (5) has the following form in the coordinate notation:

$$\begin{cases} \frac{dm_x}{d\tau} = (m_z f_y - m_y f_z) + \alpha f_x - \alpha m_x L, \\ \frac{dm_y}{d\tau} = (m_x f_z - m_z f_x) + \alpha f_y - \alpha m_y L, \\ \frac{dm_z}{d\tau} = (m_y f_x - m_x f_y) + \alpha f_z - \alpha m_z L, \end{cases} \quad (6)$$

where

$$L = (\mathbf{m}, \mathbf{f}) = km_x^2 + hm_x - bjm_y - m_z^2.$$

Its expanded coordinate view is written below (cf. with the dynamical system for STT-MRAM with longitudinal anisotropy [12,13]):

$$\begin{aligned} \frac{dm_x}{d\tau} &= \tilde{P}(m_x, m_y, m_z) = -bjm_z + bjm_x m_y + m_y m_z \\ &+ a(h + km_x + bjm_z - hm_x^2 - km_x^3 + bjm_x m_y + m_x m_z^2), \end{aligned}$$

$$\begin{aligned} \frac{dm_y}{d\tau} &= \tilde{Q}(m_x, m_y, m_z) = -bjm_x - m_x m_z - hm_z - km_x m_z \\ &- bjm_z^2 + a(m_y m_z^2 - hm_x m_y - km_y m_x^2 - bjm_x^2 - bjm_z^2), \end{aligned}$$

$$\begin{aligned} \frac{dm_z}{d\tau} &= \tilde{S}(m_x, m_y, m_z) = hm_y + km_x m_y + bjm_y m_z + bjm_x \\ &+ a(bjm_y m_z + m_z^3 - bjm_x - m_z - hm_x m_z - km_x^2 m_z). \end{aligned} \quad (7)$$

Just as in the case of STT-MRAM, the system (7) has the first integral and is a system with two degrees of freedom. When $h = 0$, $j = 0$ when the field and current are disconnected, the system (7) degenerates to form

$$\begin{aligned} \frac{dm_x}{d\tau} &= \tilde{P}_0(m_x, m_y, m_z) = m_y m_z + a(km_x - km_x^3 + m_x m_z^2), \\ \frac{dm_y}{d\tau} &= \tilde{Q}_0(m_x, m_y, m_z) = -m_x m_z - km_x m_z \\ &+ a(m_y m_z^2 - km_y m_x^2), \\ \frac{dm_z}{d\tau} &= \tilde{S}_0(m_x, m_y, m_z) = km_x m_y + a(m_z^3 - m_z - km_x^2 m_z). \end{aligned} \quad (8)$$

Its singular points (equilibrium points) are points $T_{1,2}(\pm 1, 0, 0)$, $T_{3,4}(0, 0, \pm 1)$, $T_{5,6}(0, \pm 1, 0)$: points $T_{1,2}$ are stable foci, points $T_{3,4}$ — unstable foci, $T_{5,6}$ — saddles. However, unlike the case of STT with nonzero currents and fields, the points $T_{1,2}(\pm 1, 0, 0)$ are not equilibrium positions of the magnetization vector of the free layer (they are not singular points of the dynamical system). The points T_{3-6} change their position depending on the control parameters. The equation for determining m_x (x -coordinates singular points) is obtained by equating the right parts of the system to zero (7) and sequentially excluding from it the variables m_y and m_z :

$$\sum_{i=0}^6 A_{6-i} m_x^{6-i} = 0, \quad (9)$$

where

$$\begin{aligned} A_6 &= (k + 1)^2 (b^2 j^2 - k)^2, \\ A_5 &= 2h(k + 1)(b^2 j^2 - 2k - 1)(b^2 j^2 - k), \\ A_4 &= 4b^2 j^2 k - k^2 + 6kh^2 - 4b^4 j^4 + b^2 j^2 - 4kb^4 j^4 - 2k^3 \\ &+ 5k^2 b^2 j^2 - k^4 + 6k^2 h^2 + h^2 - 4h^2 b^2 j^2 + 2k^3 b^2 j^2 \\ &+ h^2 b^4 j^4 - 6kh^2 b^2 j^2, \\ A_3 &= -2h(-2b^2 j^2 + 3k^2 - 2kh^2 + k - 5kb^2 j^2 - 3k^2 b^2 j^2 \\ &+ 2b^4 j^4 + 2k^3 - h^2 + h^2 b^2 j^2), \\ A_2 &= -6kh^2 - 2kb^4 j^4 - 6k^2 h^2 + 4b^6 j^6 + h^4 + 5h^2 b^2 j^2 \\ &+ 6kh^2 b^2 j^2 + k^2 b^2 j^2 - k^2 b^4 j^4 - b^4 j^4 - h^2, \\ A_1 &= -2h(h^2 + 2kh^2 - h^2 b^2 j^2 - kb^2 j^2 + b^4 j^4 + kb^4 j^4), \\ A_0 &= -h^2(h^2 - b^2 j^2 + b^4 j^4). \end{aligned}$$

Note here the symmetry of the coefficients A_{1-6} with respect to the parameter j and their antisymmetry relative to h . In other words, the sign of the magnitude m_x will change when the direction of the field changes h , i.e., the

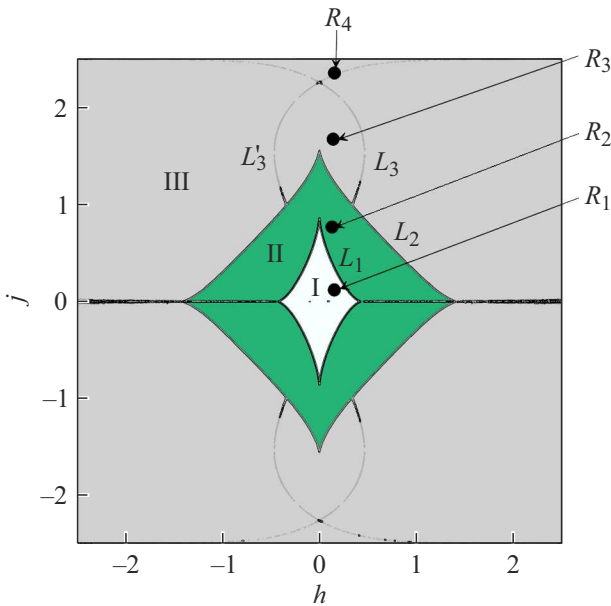


Figure 2. Distribution of the number of singular points on the plane of control parameters „field–current“: in region I singular points six, in region II — four, in region III — two.

location of the singular point relative to the zero meridian will change. This is essential when the trailing edge of the control pulse travels, as it indicates which equilibrium attraction pool the trajectory of the end of the magnetization vector on a unit sphere will fall into.

Further, m_z and m_y is calculated, for example, from the following intermediate relations after determining from (9) the coordinate m_x of the magnetization vector:

$$m_z = -bj r_1/r_2 \quad (m_x \neq 0, h \neq 0),$$

where

$$r_1 = (k^2 - 1)m_x^4 + 2hkm_x^3 + (2b^2j^2 + h^2 - k^2)m_x^2 - 2hkm_x - h^2,$$

$$r_2 = (k + 1)(b^2j^2 - 1)m_x^3 + h(b^2j^2 - 1)m_x^2 - (k - 1)b^2j^2m_x - hb^2j^2,$$

and

$$m_y = -r_3/r_4,$$

where

$$r_3 = am_xm_z^2 - (1 - a)bjm_z + a(km_x + h)(1 - m_x^2),$$

$$r_4 = m_z - (a + 1)bjm_x.$$

Two singular points with coordinates $(0, -bj, +\sqrt{1-b^2j^2})$ and $(0, +bj, -\sqrt{1-b^2j^2})$ are found by direct substitution in (7) if simultaneously $m_x = 0$ and $h = 0$.

The diagram of the distribution of the number of singular points on the plane of the control parameters „field–current“ is shown in Fig. 2. The methods of Sturm and Laguerre were used for calculations [15]. Two nested rhombus-like regions can be distinguished depending on the magnitude of the field and current on the plane: equation (9) has six real roots in the region I (Fig. 3) satisfying the condition $|m_x| \leq 1$; there are four real roots in region II (Fig. 4), there are two real roots in region III (Fig. 5). These roots correspond to a pair of foci in region III such as stable and unstable (see Table. 1 and Fig. 5). On lines L_1, L_2, L_3, L_4 imaginary parts of the eigenvalues of the linearization matrix of the system (7) turn to zero. The corresponding singular point becomes a node. The direction of rotation of the trajectory of the end of the magnetization vector around a singular point changes when the control parameters pass through these lines. There are four singular points in region II — two unstable foci, a stable focus and a saddle, there are six singular points in region I two stable and two unstable foci, and two saddles. Table 1 shows the coordinates of singular points T_{1-6} in the regions I–III of the bifurcation diagram at three characteristic points R_1 ($h = 0.1, j = 0.1$), R_2 ($h = 0.1, j = 0.8$), R_3 ($h = 0.1, j = 1.5$) and the corresponding eigenvalues of a dynamical system linearized in the neighborhood of each of the points T_{1-6} :

$$\begin{aligned} dm_x/d\tau &\approx P(m_{x_0}, m_{y_0}, m_{z_0}) + \partial P/\partial m_x|_{T_0}(m_x - m_{x_0}) \\ &\quad + \partial P/\partial m_y|_{T_0}(m_y - m_{y_0}) + \partial P/\partial m_z|_{T_0}(m_z - m_{z_0}), \\ dm_y/d\tau &\approx Q(m_{x_0}, m_{y_0}, m_{z_0}) + \partial Q/\partial m_x|_{T_0}(m_x - m_{x_0}) \\ &\quad + \partial Q/\partial m_y|_{T_0}(m_y - m_{y_0}) + \partial Q/\partial m_z|_{T_0}(m_z - m_{z_0}), \\ dm_z/d\tau &\approx S(m_{x_0}, m_{y_0}, m_{z_0}) + \partial S/\partial m_x|_{T_0}(m_x - m_{x_0}) \\ &\quad + \partial S/\partial m_y|_{T_0}(m_y - m_{y_0}) + \partial S/\partial m_z|_{T_0}(m_z - m_{z_0}). \end{aligned}$$

3. Numerical results

The results of simulation the magnetization dynamics for positive current and field are shown in Fig. 6 and in Fig. 7 for $(j, h) < 0$. A stable focus is marked T_6 on Fig. 6 with coordinates on the unit sphere $m_x = 0.24206, m_y = -0.96612, m_z = -8.9564 \cdot 10^{-2}$. The second singular point is an unstable focus T_5 with coordinates $m_x = 0.21749, m_y = 0.76427, m_z = -0.60712$ is not shown in Fig. 6. A single trajectory passes through any regular point on the sphere, which begins in an unstable focus and ends in a stable one. The trajectories which are equilibrium positions in the case of zero fields and currents passing through the points $T_{1,2}(\pm 1, 0, 0)$ are important for switching the SOT-MRAM element. The trajectories leaving the points T_1 (Fig. 6, a) or T_2 (Fig. 6, b) end in point T_6 with a positive current (blue trajectories on the unit sphere). If the current is turned off (a current pulse of finite duration is applied

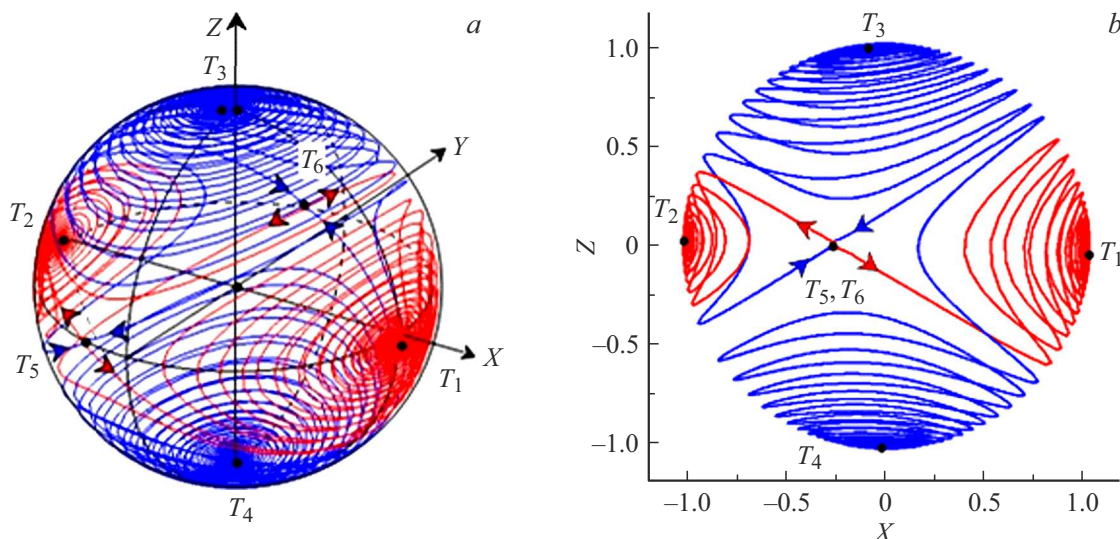


Figure 3. *a* — phase surface of a dynamical system (7) in the region I of the bifurcation diagram Fig. 2 ($h = 0.1, j = 0.1$). Points T_1, T_2 — stable foci, T_3, T_4 — unstable foci, T_5, T_6 — saddles); *b* — projections of saddle separatrix to plane XZ.

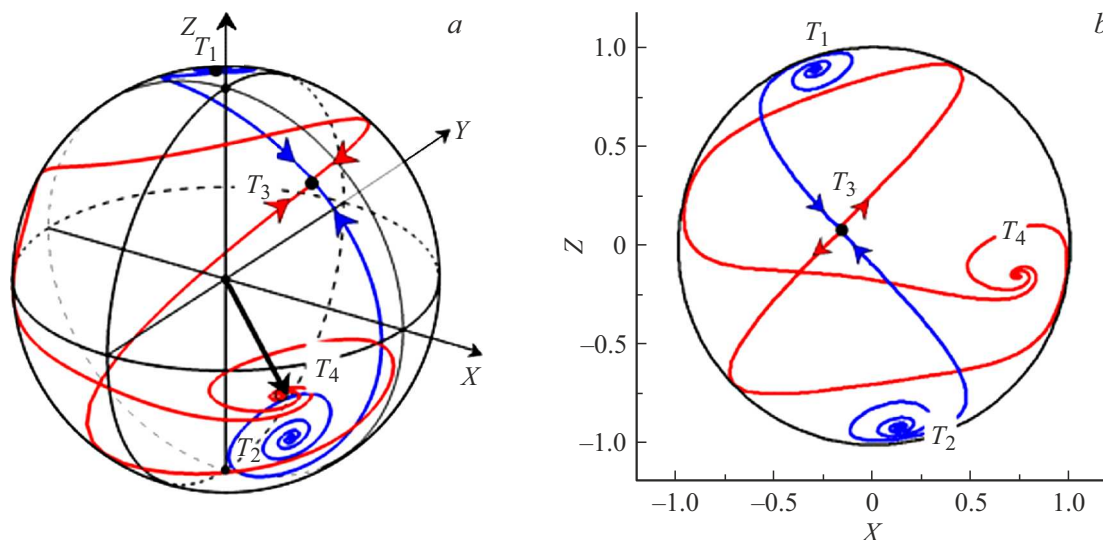


Figure 4. Phase portrait of the dynamical system (7) in the region II of the bifurcation diagram Fig. 2: *a* — the separatrices of the saddle on the surface of the unit sphere, *b* — projections of the separatrices on the plane XZ.

to the element), then the equilibrium will disappear at the point T_6 , but six new equilibria will appear, two of which — $T_{1,2}$ — will be stable. The point T_6 will become regular and fall into the basin of attraction of one of the new equilibrium positions for the new dynamical system $T_{1,2}(\pm 1, 0, 0)$. On the sphere, this corresponds to a spiral trajectory that begins at the former equilibrium point T_6 and ends at the new stable equilibrium point $T_1(1, 0, 0)$. Thus, either the cell switches from the position „unit“ to the position „zero“ (Fig. 6, *a*), or returns from zero to the previous position $T_1(1, 0, 0)$ (Fig. 6, *b*). In the case of negative field and current pulses, the stable equilibrium position corresponds to the point T_5 , which is located in the opposite hemisphere, the attraction basins change places and the reverse switching

occurs from „zero“ to „unit“ (Fig. 7, *a*). If the initial position was „unit“, then after switching off the current and the field, the magnetization vector returns to the initial position „zero“ (Fig. 7, *b*). Switching is impossible in the region I because singular points of the perturbed system here (7) are small deviations of the undisturbed system (8), so that when external impacts are turned off, the magnetization vector will return to its original position.

4. Critical currents and switching fields

The rhombus-like form of the regions of equivalent dynamics on the plane „field–current“ allows estimating the critical currents and fields required to switch SOT-MRAM

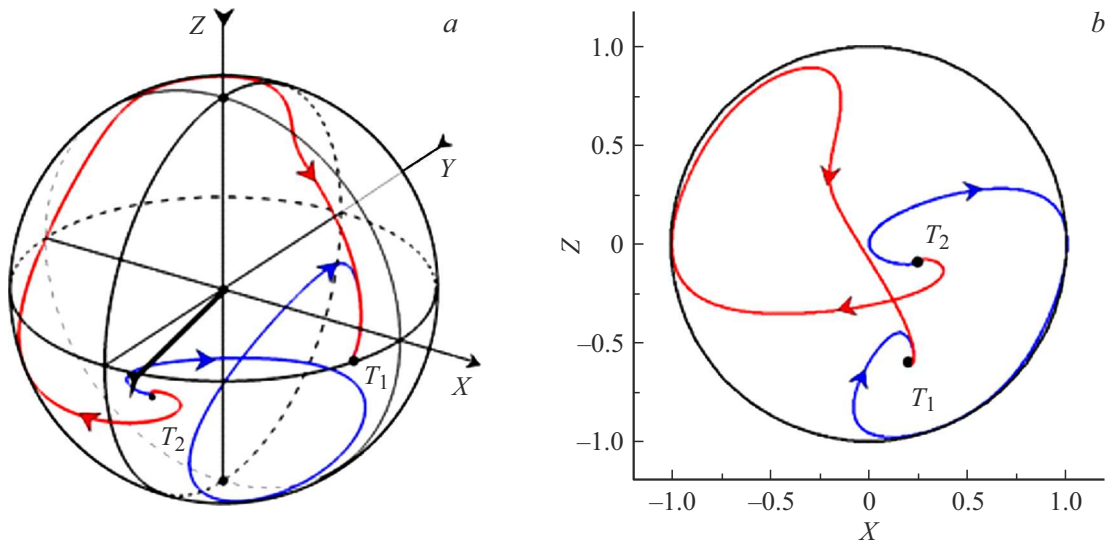


Figure 5. Phase portrait of a dynamic system (7) in the region III of the bifurcation diagram Fig. 2: *a* — trajectories on the surface of a unit sphere, *b* — projection of trajectories onto plane XZ. Note: one and only one phase trajectory passes through each regular point of the sphere, but since the phase surface of the system itself is ambiguous, trajectories located on different hemispheres of the sphere when projected onto a plane may have intersection points, which is observed in Fig. 3–5.

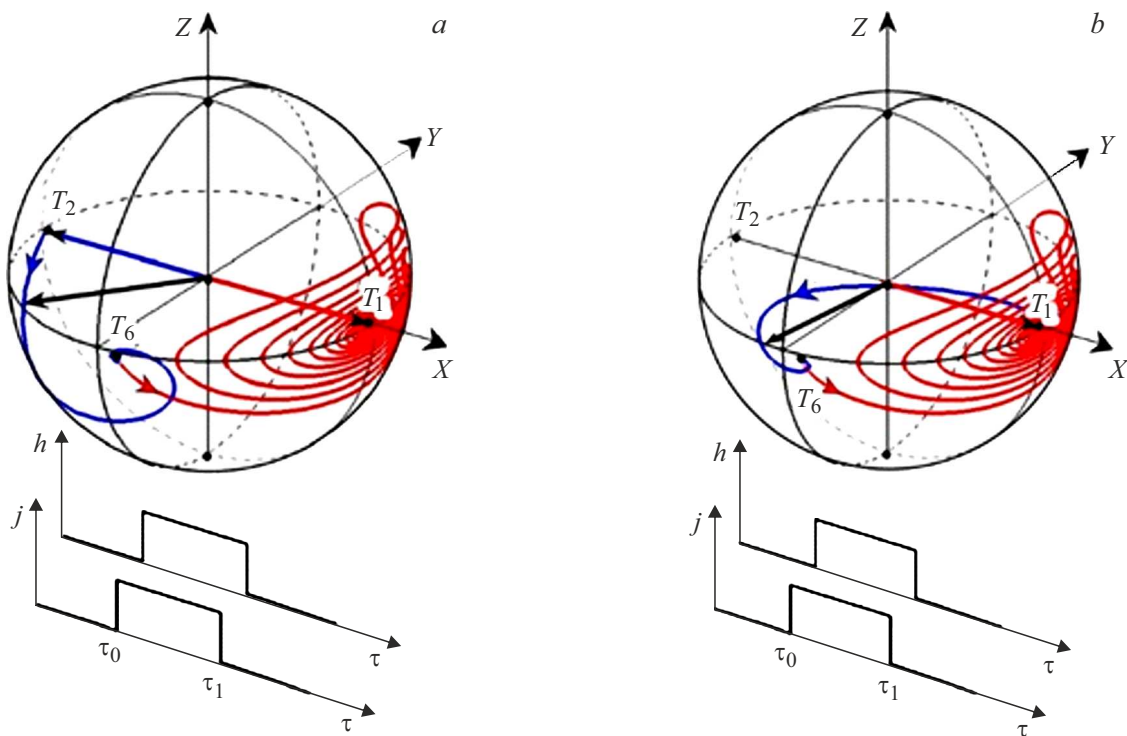


Figure 6. Hodographs of the vector \mathbf{m} originating from the equilibrium positions $T_1(1, 0, 0)$ (*a*) and $T_2(-1, 0, 0)$ (*b*) under the action of positive magnetic field pulses and current (blue lines (in online version)) and the trajectories of the end of the magnetization vector at $j, h = 0$ (red lines (in online version)).

cells from one equilibrium position to another. Let's put the value of the field $h = 0$ In this case equation (9) can be written as follows

$$m_x^2 (B_4 m_x^4 + B_2 m_x^2 + B_0) = 0, \tag{10}$$

where

$$B_4 = (k + 1)^2 (k - b^2 j^2)^2,$$

$$B_2 = -(k + 1)(k^3 - 2b^2 j^2 k^2 + k^2 - 3b^2 j^2 k - b^2 j^2 + b^4 j^4),$$

$$B_0 = -b^2 j^2 (b j k - k - b j + 2b^2 j^2)(b j k + k - b j - 2b^2 j^2).$$

Table 1. Coordinates and types of singular points on a spherical phase surface at a positive current pulse

| Control parameters | Coordinates of singular points and eigenvalues of the matrix Dynamical system linearization (7) | Point type |
|---------------------------------------|--|------------|
| Region I $R_1(h = 0.1, j = 0.1)$ | $T_1(0.997, -0.076, -0.026):$ $\lambda_1 = -0.024 + 0.897i, \lambda_2 = -0.024 - 0.897i, \lambda_3 = -0.021$ | SF |
| | $T_2(-0.992, -0.123, 0.003):$ $\lambda_1 = 0.011 + 0.649i, \lambda_2 = -0.011 - 0.649i, \lambda_3 = -0.013$ | SF |
| | $T_3(-0.098, 0.040, 0.994):$ $\lambda_1 = 0.026 + 1.185i, \lambda_2 = 0.026 - 1.185i, \lambda_3 = 0.039$ | USF |
| | $T_4(-0.042, 0.040, -0.998):$ $\lambda_1 = 0.026 + 1.195i, \lambda_2 = 0.026 - 1.195i, \lambda_3 = 0.040$ | USF |
| | $T_5(-0.213, 0.977, 0.009):$ $\lambda_1 = 0.692, \lambda_2 = -0.624, \lambda_3 = 0.0001$ | Saddle |
| | $T_6(-0.258, -0.996, 0.010):$ $\lambda_1 = -0.658, \lambda_2 = 0.567, \lambda_3 = 0.0001$ | Saddle |
| Region II $R_2(h = 0.1, j = 0.8)$ | $T_1(-0.290, 0.357, 0.888):$ $\lambda_1 = 0.134 + 0.951i, \lambda_2 = 0.134 - 0.951i, \lambda_3 = 0.031$ | USF |
| | $T_2(0.143, 0.337, -0.931):$ $\lambda_1 = 0.129 + 1.06i, \lambda_2 = 0.129 - 1.06i, \lambda_3 = 0.034$ | USF |
| | $T_3(-0.165, 0.983, 0.008):$ $\lambda_1 = 1.021, \lambda_2 = -0.390, \lambda_3 = 0.0001$ | Saddle |
| | $T_4(0.747, -0.645, -0.159):$ $\lambda_1 = -0.224 + 0.669i, \lambda_2 = -0.224 - 0.669i, \lambda_3 = -0.011$ | SF |
| Region III $R_3(h = 0.1, j = 1.5)$ | $T_1(0.217, 0.764, -0.607):$ $\lambda_1 = 0.472 + 0.422i, \lambda_2 = 0.472 - 0.422i, \lambda_3 = 0.013$ | USF |
| | $T_2(0.242, -0.966, -0.009):$ $\lambda_1 = -0.598 + 0.572i, \lambda_2 = -0.598 - 0.572i, \lambda_3 = -0.002$ | SF |
| Region III $R_4(h = 0.1, j = 2.5)$ | $T_1(-4.9312 \cdot 10^{-4}, 0.99532, -9.9292 \cdot 10^{-2}):$ $\lambda_1 = 1.0979, \lambda_2 = 0.92173, \lambda_3 = 3.987 \cdot 10^{-4}$ | USN |
| | $T_2(9.3102 \cdot 10^{-2}, -0.99455, -4.6422 \cdot 10^{-2}):$ $\lambda_1 = -1.0204 + 1.0531i, \lambda_2 = -1.0204 - 1.0531i, \lambda_3 = -4.3593 \cdot 10^{-4}$ | SF |

Note. Designations of the types of singular points: SF — stable focus, USF — unstable focus, SN — stable node, USN — unstable node.

Thus, the polynomial (10) always has at least two real multiples of the root for $h = 0$. There are also two or four real roots that nullify a fourth-degree trinomial in (10). For this, the following two conditions should be met:

1. $D = B_2^2 - 4B_0B_4 \geq 0,$
2. $0 \leq \frac{-B_2 \pm \sqrt{D}}{2B_0} \leq 1.$

The first condition is met in the interval $|j| \leq (k + 1)/(2b)$. The left part of the second inequality is valid in the range of positive currents

$$(k - 1 + \sqrt{k^2 + 6k + 1})/(4b) \leq j \leq (-k + 1 + \sqrt{k^2 + 6k + 1})/(4b)$$

and in a symmetrical range of negative currents

$$(k - 1 - \sqrt{k^2 + 6k + 1})/(4b) \leq j \leq (-k + 1 - \sqrt{k^2 + 6k + 1})/(4b).$$

The right part is always fulfilled when the previous conditions are met (if a solution (10) exists, then it is modulo less than one).

For $j = 0$ the equation (9) is reduced to the equation

$$(1 - m_x^2)(km_x + h)^2[(k + 1)m_x + h]^2 = 0. \tag{11}$$

There is also always a pair of roots $m_x = \pm 1$ and two pairs of multiple roots at intervals $|h| \leq k$ and $|h| \leq k + 1$. Thus, in the first quarter of the plane of the control parameters „the field–current“ can be constructed two straight lines approximating the critical lines L_1 and L_2 separating the regions of existence of the system (7): six, four and two special points

$$L'_1: \frac{4bj}{k - 1 + \sqrt{k^2 + 6k + 1}} + \frac{h}{k} = 1,$$

$$L'_2: \frac{4bj}{-k + 1 + \sqrt{k^2 + 6k + 1}} + \frac{h}{k + 1} = 1. \tag{12}$$

The symmetry property of the problem can be used in the remaining quarters. Formulas (12) allow estimating the

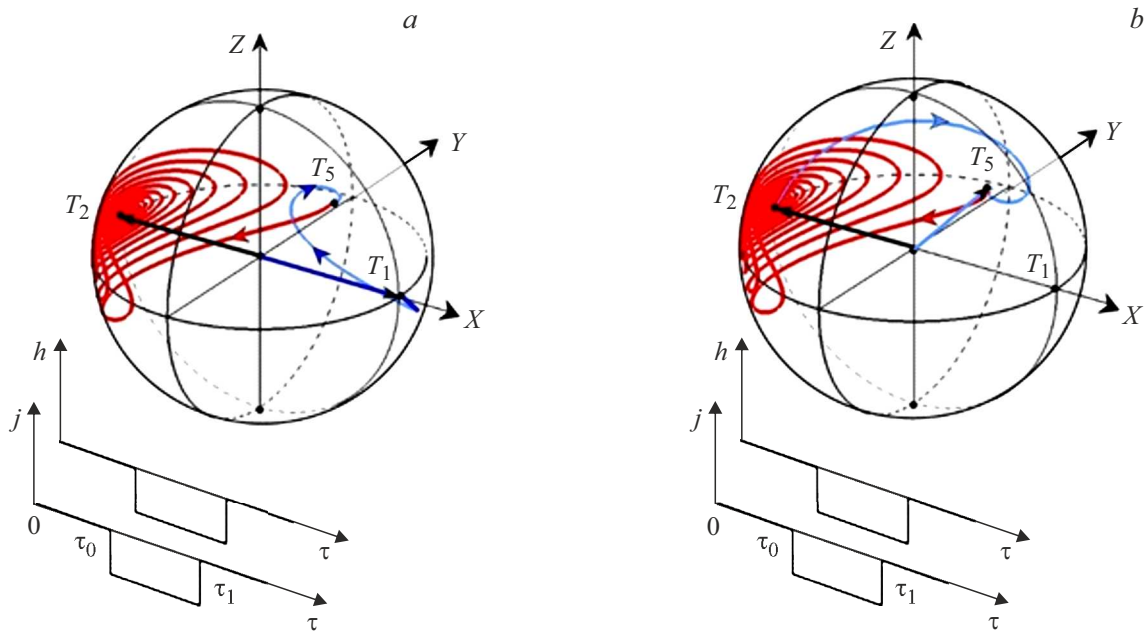


Figure 7. Trajectories of the end of the magnetization vector originating from the points $T_1(1, 0, 0)$ (a) and $T_2(-1, 0, 0)$ (b) under the action of pulses of a negative magnetic field and current (blue lines (in online version)) and trajectories of the end of the magnetization vector at zero currents and fields (red lines (in online version)).

Table 2. Values of maximum switching currents of three-layer SOT-MRAM structures through a square cross section $S = 10 \times 10 \text{ nm}$ ([19-21])

| Structure | $k = \frac{2K}{\mu_0 M_s^2}$ | j_1 | j_2 | I_1 (A) | I_2 (A) |
|---|------------------------------|-----------------------|-------|------------------------|-----------------------|
| Pt/Co/MgO | 0.43 | 0.856 | 1.569 | $1.388 \cdot 10^{-3}$ | $2.542 \cdot 10^{-3}$ |
| Pt/Fe/MgO | $2.61 \cdot 10^{-2}$ | $6.36 \cdot 10^{-2}$ | 1.281 | $1.539 \cdot 10^{-4}$ | $3.098 \cdot 10^{-3}$ |
| Pt/Fe ₇₀ Co ₃₀ /MgO | $1.53 \cdot 10^{-2}$ | $3.76 \cdot 10^{-2}$ | 1.268 | $1.134 \cdot 10^{-4}$ | $3.822 \cdot 10^{-3}$ |
| Pt/Fe ₆₀ Co ₂₀ B ₂₀ /MgO | 0.137 | 0.309 | 1.388 | $6.218 \cdot 10^{-4}$ | $2.789 \cdot 10^{-3}$ |
| Pt/Fe ₄₀ Co ₄₀ B ₂₀ /MgO | $5.056 \cdot 10^{-8}$ | $1.264 \cdot 10^{-7}$ | 1.250 | $1.118 \cdot 10^{-10}$ | $1.105 \cdot 10^{-3}$ |

switching current densities depending on the magnitude of the applied magnetic field.

Note: transition from dimensionless to dimensional quantities:

$$k = \frac{2K}{\mu_0 M_s^2}, \quad j_1 = \frac{k - 1 + \sqrt{k^2 + 6k + 1}}{4b},$$

$$j_2 = \frac{-k + 1 + \sqrt{k^2 + 6k + 1}}{4b},$$

$$J_1 = j_1 \frac{dg|e|\mu_0 M_s^2}{g\hbar} \text{ (A/m}^2\text{)}, \quad J_2 = j_2 \frac{dg|e|\mu_0 M_s^2}{\hbar} \text{ (A/m}^2\text{)},$$

$$I_1 = J_1 S \text{ (A)}, \quad I_2 = J_2 S \text{ (A)}.$$

Conclusion

A model of a SOT-MRAM magnetic memory element with a longitudinal anisotropy of the free layer and with an

external field parallel to the anisotropy field was constructed and studied in this paper. Stoner–Wohlfarth approximation made it possible to reduce the problem of describing the dynamics of magnetization to the analysis of a dynamical system with two degrees of freedom. Such a system can be analyzed by the methods of the qualitative theory of dynamical systems. The number and type of its singular points is an important characteristic of the system in this context [16–18]. The direct application of known methods of numerical solution of algebraic nonlinear systems for finding them numerically often leads to unsatisfactory results [15]. A more effective approach is to reduce the system of equations to a single polynomial type equation, for which numerical methods provide a proven and reliable solution path. Finding singular points of the system (equilibrium states) made it possible to classify the dynamic modes in the MRAM cell and the types of phase trajectories of the end of the magnetization vector on a spherical phase

surface. Previously, we used such an analysis to describe the dynamics of magnetization in STT-MRAM [12–14] elements. In our calculations, we used numerical values of the physical quantities from papers [19–21] (Table 2).

Conflict of interest

The authors declare that they have no conflict of interest.

References

- [1] B. Dieny, I.L. Prejbeanu, K. Garello, P. Gambardella, P. Freitas, R. Lehdorf, W. Raberg, U. Ebels, S.O. Demokritov, J. Akerman, A. Deac, P. Pirro, C. Adelmann, A. Anane, A.V. Chumak, A. Hirohata, S. Mangin, S.O. Valenzuela, M. Cengiz-Onbasli, M. d’Aquino, G. Prenat, G. Finocchio, L. Lopez-Diaz, R. Chantrell, O. Chubykalo-Fesenko, P. Bortolotti. *Nature Electron.*, **3** (8), 446 (2020). DOI: 10.1038/s41928-020-0461-5
- [2] F. Hellman, A. Hoffmann, Ya. Tserkovnyak, G.S.D. Beach, E.E. Fullerton, C. Leighton, A.H. MacDonald, D.C. Ralph, D.A. Arena, H.A. Durr, P. Fischer, J. Grollier, J.P. Heremans, T. Jungwirth, A.V. Kimel, B. Koopmans, I.I. Krivorotov, S.J. May, A.K. Petford-Long, J.M. Rondinelli, N. Samarth, I.K. Schuller, A.N. Slavin, M.D. Stiles, O. Tchernyshyov, A. Thiaville, B.L. Zink. *Rev. Modern Phys.*, **89** (2), 025006 (2017). DOI: 10.1103/RevModPhys.89.025006
- [3] Ch.-F. Pai, L. Liu, Y. Li, H.W. Tseng, D.C. Ralph, R.A. Buhrman. *Appl. Phys. Lett.*, **101**, 122404 (2012). DOI: 10.1063/1.4753947
- [4] Ch. Song, R. Zhang, L. Liao, Y. Zhou, X. Zhou, R. Chen, Y. You, X. Chen, F. Pan. *Progress Mater. Sci.*, **118** (5), 100761 (2021). DOI: 10.1016/j.pmatsci.2020.100761
- [5] Y. Wang, P. Deorani, X. Qiu, J.H. Kwon, H. Yang. *Appl. Phys. Lett.*, **105**, 152412 (2014). DOI: 10.1063/1.4898593
- [6] Y. Deng, M. Yang, Y. Ji, K. Wang. *JMMM*, **496** (2), 165920 (2020). DOI: 10.1016/j.jmmm.2019.165920
- [7] S. Fukami, T. Anekawa, C. Zhang, H. Ohno. *Nature Nanotechnology*, **11** (3), 621 (2016). DOI: 10.1038/NNANO.2016.29
- [8] L.D. Landau, E.M. Lifshitz. *K teorii dispersii magnitnoy pronitsaemosti ferromagnitnykh tel, v Sobranii trudov L.D. Landau* (Nauka, M., 1969), vol. 1, p. 128 (in Russian).
- [9] T.L. Gilbert. *IEEE Transactions on Magnetics*, **40** (6), 3443 (2004). DOI: 10.1109/TMAG.2004.836740
- [10] Y.-T. Liu, T.-Y. Chen, T.-H. Lo, T.-Y. Tsai, Sh.-Y. Yang, Y.-J. Chang, J.-H. Wei, Ch.-F. Pai. *Phys. Rev. Appl.*, **13**, 044032 (2020). DOI: 10.1103/PhysRevApplied.13.044032
- [11] J. Slonczewskii. *JMMM*, **159**, L1 (1996). DOI: 10.1016/0304-8853(96)00062-5
- [12] N.V. Ostrovskaya, V.A. Skidanov, Yu.A. Yusipova. *Komp’yuternye issledovaniya i modelirovaniye*, **8** (4), 605 (2016) (in Russian). DOI: 10.20537/2076-7633-2016-8-4-605-620
- [13] N.V. Ostrovskaya, Yu.A. Iusipova. *Phys. Metals and Metallography*, **120** (13), 1291 (2019). DOI: 10.1134/S0031918X19130209
- [14] N.V. Ostrovskaya, V.A. Skidanov. V sb.: *Problemy razrabotki perspektivnykh mikro- i nanoelektronnykh sistem*, pod red. A.L. Stempkovsky (Moscow, Zelenograd, 2020), vol. III, p. 127 (in Russian). DOI: 10.31114/2078-7707-2020-3-127-132
- [15] S.A. Teukolsky, W.T. Vetterling, B.P. Flannery, W.H. Press. *Numerical Recipes: The art of Scientific Computing*, 3rd ed., (Cambridge University Press, Cambridge–NY–Melbourne–Madrid–Cape Town–Singapore–San Paulo, 2007)
- [16] J. Guckenheimer, Ph. Holmes, *Nonlinear Oscillations, Dynamical Systems, and Bifurcations of Vector Fields* (Appl. Mathemat. Sci., Springer–Verlag, 6th cor. ed., NY, 2002), v. 42.
- [17] N.N. Bautin, E.A. Leontovich, *Methody i priemy kachestvennogo issledovaniya dinameskikh sistem na ploskosti*, SMB (Nauka, M., 1990) (in Russian)
- [18] A.A. Andronov, E.A. Leontovich, I.I. Gordon, A.G. Mayer. *Kachestvennaya teoriya sistem vtorogo poriyadka* (Nauka, M., 1966) (in Russian)
- [19] Yu.A. Iusipova. *Semiconductors*, **52** (15), 1982 (2018). DOI: 10.1134/S1063782618150162
- [20] X. Han, X. Wang, C. Wan, G. Yu, X. Lv. *Appl. Phys. Lett.*, **118**, 120502 (2021). DOI: 10.1063/5.0039147
- [21] A.T. Hindmarch, A.W. Rushforth, R.P. Champion, C.H. Marrows, B.L. Gallagher. *Phys. Rev. B*, **83**, 212404 (2011). DOI: 10.1103/PhysRevB.83.212404

Translated by A.Akhtyamov